Low depinning fields in Ta-CoFeB-MgO ultrathin films with perpendicular magnetic anisotropy

C. Burrowes,[1,2] N. Vernier,[1,2] J.-P. Adam,[1,2] L. Herrera Diez,[1,2] K. Garcia,[1,2] I. Barisic,[1,2]
G. Agnus,[1,2] S. Eimer,[1,2] Joo-Von Kim,[1,2] T. Devolder,[1,2] A. Lamperti,[3] R. Mantovan,[3]
B. Ockert,[4] E. E Fullerton,[5] and D. Ravelosona[1,2]

[1]*Institut d'Electronique Fondamentale, Université Paris-Sud, 91405 Orsay, France*
[2]*UMR CNRS 8622, 91405 Orsay, France*
[3]*Laboratorio MDM, IMM-CNR, Via C. Olivetti 2, 20864 Agrate Brianza (MB), Italy*
[4]*Singulus Technology AG, Hanauer Landstrasse 103, 63796 Kahl am Main, Germany*
[5]*Center for Magnetic Recording Research, University of California San Diego, San Diego, 92093-0401 California, USA*

We have studied the domain-wall dynamics in Ta-CoFeB-MgO ultra-thin films with perpendicular magnetic anisotropy for various Co and Fe concentrations in both the amorphous and crystalline states. We observe three motion regimes with increasing magnetic field, which are consistent with a low fields creep, transitory depinning, and high fields Walker wall motion. The depinning fields are found to be as low as 2 mT, which is significantly lower than the values typically observed in 3d ferromagnetic metal films with perpendicular magnetic anisotropy. This work highlights a path toward advanced spintronics devices based on weak random pinning in perpendicular CoFeB films.

One promising application in spintronics is the magnetic shift memory,[1,2] which involves the propagation of multiple magnetic domain walls in magnetic tracks under the action of an electrical current rather than an applied magnetic field. In this context, the use of materials with perpendicular magnetic anisotropy (PMA) is actively pursued. The large anisotropy values in such materials yields narrow domain walls (~10–20 nm typically) making them good candidates for high-density magnetic storage. However, in ultrathin film or multilayers exhibiting PMA, these narrow domain walls (DWs) interacts very strongly with a distribution of random nanoscale inhomogeneties present in thin films.[3] The competition between the elasticity of the DW and pinning to the local disorder leads to a thermally activated creep motion for $H \ll H_{dep}$, where H_{dep} is the depinning field. For fields beyond H_{dep}, the DW moves in a viscous flow regime where the pinning vanishes.[4] In this regime, the 1D model of Schryer and Walker[5] predicts a steady and precessional linear regime separated by an intermediate regime dominated by the Walker breakdown with negative DW mobility. In typical films with PMA such as Co/Pt,[4] Co/Ni,[6] or FePt,[7] the depinning field H_{dep} is generally very large (>20 mT typically), which not only amplifies stochastic effects over a wide range of fields[8,9] but can lead to high threshold currents for current-induced wall motion, which is detrimental for future applications.[10–12]

Recent studies have shown that CoFeB alloys, an amorphous soft magnetic material that crystallizes into the bcc structure after annealing at temperature around 300 °C, exhibits strong PMA when grown as an ultrathin film on a Ta buffer layer and capped with MgO.[13] This material combination has been widely studied in magnetic tunnel junctions with in plane anisotropy because of the high spin polarization of CoFeB and the relatively large tunneling magnetoresistance (TMR) ratios of CoFeB/MgO/CoFeB structures.[14] The presence of an amorphous (and subsequently fully crystallized

bcc phase) may be expected to lead to a low density of structural defects with respect to conventional fcc textured 3d ferromagnetic metals with PMA such as Co/Ni, Co/Pd, or Co/Pt multilayers,[4,6] which is favorable for DW motion. In most studies to date, however, the magnetization dynamics of CoFeB materials with PMA has been mostly limited to current perpendicular to the plane nanopillars.[13] Owing to the additional potential of using TMR through the MgO layer to detect domain wall motion, CoFeB-MgO structures show promise as material in high performance racetrack memory. Particularly, a recent study has shown that DWs can move under relatively low current densities in Ta-$Co_{20}Fe_{60}B_{20}$-MgO wires.[15]

Here, we report on domain wall dynamics under fields in Ta-CoFeB-MgO films with PMA that exhibits very low depinning fields. The studied samples consist of Ta(5 nm)/CoFeB (1 nm)/MgO(2 nm)/Ta(5 nm) multilayered thin films. Three different combinations of Co and Fe concentrations considered are $Co_{20}Fe_{60}B_{20}$, $Co_{40}Fe_{40}B_{20}$, and $Co_{60}Fe_{20}B_{20}$. The layers, grown on Si(001)/300 nm-SiO_2 substrates by sputtering at room temperature, using a TIMARIS *Singulus* tool, remained highly homogeneous over 8 inches, in terms of both thicknesses and PMA properties.[16,17] The samples with compositions $Co_{20}Fe_{60}B_{20}$ and $Co_{40}Fe_{40}B_{20}$ exhibit perpendicular anisotropy in the as-deposited (amorphous) state,[18] which can be seen in the hysteresis loops measured by Kerr microscopy (Figs. 1(a) and 1(b)). For samples with composition $Co_{60}Fe_{20}B_{20}$ (Figs. 1(c) and 1(d)), the as-deposited state is magnetized in the film plane but annealing at 300 °C for two h results in a film with PMA (Fig. 1(d)). Indeed, the annealing leads to an increase of the CoFeB-MgO interface anisotropy through the crystallization of the CoFeB layer into the bcc (001) phase and a chemical transformation.[13] This effect is illustrated in hysteresis loops measured in perpendicular fields becoming sharper after annealing with a slight increase of the coercive field H_c.
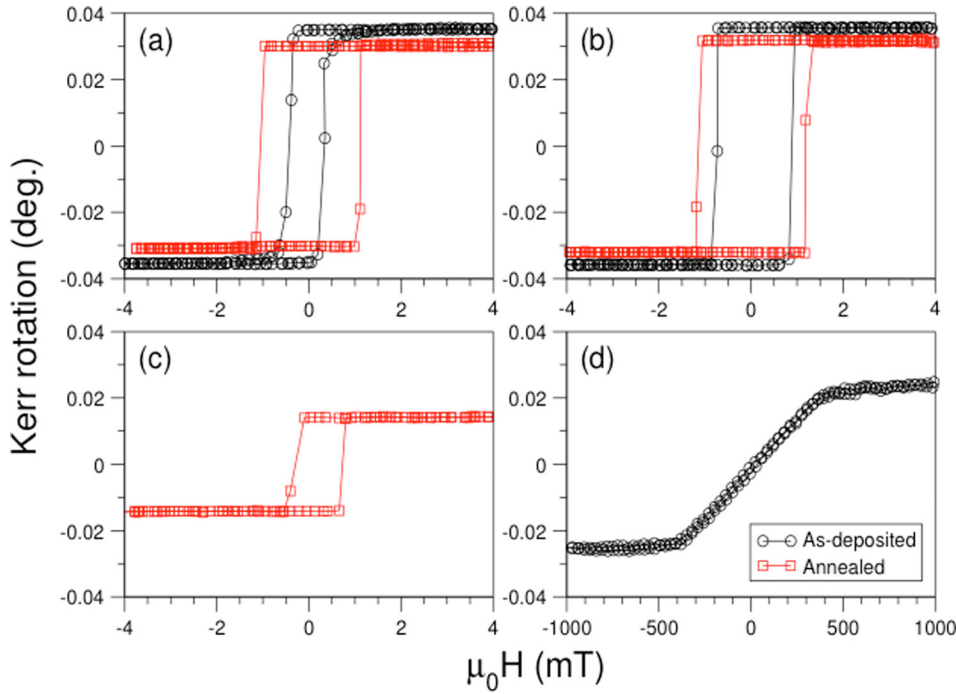
FIG. 1. Hysteresis loops measured using MOKE for different CoFeB compositions in the as-deposited and annealed states. (a) $Co_{20}Fe_{60}B_{20}$, (b) $Co_{40}Fe_{40}B_{20}$, (c) $Co_{60}Fe_{20}B_{20}$ after annealing, and (d) $Co_{60}Fe_{20}B_{20}$ as-deposited, which is in-plane magnetized.

The magnetic properties of our samples have been characterized with a number of different methods and are summarized in Table I. The saturation magnetization M_S is observed to increase upon thermal annealing, which is related to the dilution effect of M_S due to the presence of B.[19] Indeed, time of flight secondary ion mass spectrometry (ToF-SIMS) depth profiles of as deposited and annealed samples accounts for B diffusion in Ta during the annealing, while B diffusion in MgO is very limited. Also, the effective anisotropy fields, H_{Keff}, increase after annealing, with H_{Keff} being determined from hysteresis loop measurements at varying field angles (relative to the film plane) and corroborated by vector network analyzer ferromagnetic resonance (VNA-FMR) measurements. The Gilbert damping parameter, α, has been as well determined by VNA-FMR.[20]

The DW dynamics under applied magnetic fields in the CoFeB films has been investigated using magneto-optical Kerr microscopy. The magnetic field H is applied perpendicular to the film plane. A small coil (few mm in size) is used, placed close to the sample, to be able to supply to the sample short field pulses down to a few μs with amplitude up to 50 mT. An important first result is that the low coercive field of around 1 mT observed on the hysteresis loops of Fig. 1

corresponds to the nucleation field H_N of a reversed domain. Only one or two dominant nucleation sites are observed over the entire surface (2×2 mm^2) of the films, which indicates that such weak spots corresponds to extrinsic defects that weakly depend on the anisotropy of the films ($H_N \ll H_{Keff}$). The same nucleation sites are involved in the as-deposited and annealed films. Once nucleated, the DW velocity is then determined from growth of the domains to magnetic field pulses of different amplitude and duration. For a given field and pulse duration, the DW displacement is deduced from the difference between two consecutive images (i.e., by comparing the images before and after the application of the field pulse). When the fields are sufficiently large, multiple domains nucleate simultaneously at different areas in the film, which makes it difficult to quantify the wall motion. This high-field limit determines the field cut-off for the velocity curves we describe below.

Representative domain patterns are shown in Fig. 2 for the crystalline $Co_{20}Fe_{60}B_{20}$ composition. First, as seen in Fig. 2(a), a field of 1 mT is applied during 2 ms to nucleate a small reversed domain. Figures 2(b)–2(d) show then subsequent DW propagation from the small reversed domain under different fields $\mu_0H = 0.1$, 0.6, and 1 mT, respectively.

TABLE I. Measured magnetic properties (effective anisotropy μ_0H_{keff}, saturation magnetization μ_0M_s, damping parameter α extracted from Ref. 20, depinning field H_{dep}, and flow field H_{flo}) for compositions $Co_{20}Fe_{60}B_{20}$ as deposited and after annealing, $Co_{40}Fe_{40}B_{20}$ as deposited and after annealing, $Co_{60}Fe_{20}B_{20}$ after annealing. Walker fields and DW width Δ have been calculated using the 1D model and experimentally determined parameters. The exchange stiffness of CoFeB films was estimated from a stoichiometry averaging of Co and Fe constant.

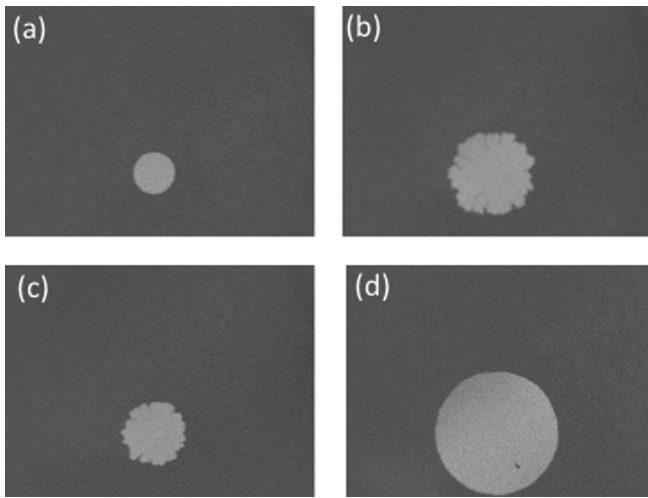|	$Co_{20}Fe_{60}B_{20}$ As-deposited	$Co_{20}Fe_{60}B_{20}$ annealed	$Co_{40}Fe_{40}B_{20}$ As-deposited	$Co_{40}Fe_{40}B_{20}$ annealed	$Co_{60}Fe_{20}B_{20}$ annealed
$\mu_0H_{k,eff}$ (mT)	45	430	107	397	82
μ_0M_S (T)	1.38	1.41	1.26	1.38	1.1
α	0.014	0.015	0.012	0.013	0.016
μ_0H_{dep} (mT)	2.5	3	2.5	3	2
μ_0H_{flo} (mT)	11	12.5	7	10	6
Δ (nm)	30.2	9.7	21	10.7	27.7
μ_0H_W (mT) theoretical	0.3	1	0.3	0.8	0.3

FIG. 2. Typical Kerr images showing domain patterns under different fields for annealed composition $Co_{20}Fe_{60}B_{20}$ (a) DW nucleation obtained at $\mu_0H = 1\,mT$, (b) DW motion under $\mu_0H = 0.1\,mT$, (c) DW motion under $\mu_0H = 0.6\,mT$, and (d) DW motion under $\mu_0H = 1\,mT$.

It is worth noting that DW propagation can be observed under fields as low as 0.1 mT. These fields are much lower than the nucleation field H_N, which explains the sharpness of the hysteresis loops. This key result suggests that the strength and the density of pinning defects in our Ta-CoFeB-MgO films are relatively low, despite the very small thickness of the magnetic material. At very low fields $\mu_0H < 0.6\,mT$, domain boundaries exhibit some jaggedness in the presence of 360° DWs, which indicates the presence of a distribution of pinning sites. However, the growth of nearly perfect circular domain at fields as low as $\mu_0H = 1\,mT$, with only minor jaggedness along the domain boundaries, suggests again the presence of very weak random pinning sites. Note that this behavior has been observed for all the samples studied here, with only a slight difference in the field at which jaggedness vanishes. The velocity curves in the low field regime are shown in logarithmic scale in Fig. 3(a). The velocity is consistent with the creep theory with velocity $\nu(H) = \nu_0 \exp(-\beta E(H))$, where $E(H) = U_c(H_{dep}/H)^{1/4}$, U_c is a scaling energy constant, H_{dep} is the depinning field, and $\beta = 1/k_BT$. Note that under the lowest fields, DW motion is more stochastic as a consequence of the presence of a distribution of pinning sites as shown in Fig. 2. Here, H_{dep} can be estimated as the average field at which DW motion leaves the creep regime (see Table I), which is between 2 and 3 mT for all samples. This is a striking result since the values for H_{dep} in Co/Pt[4] or Co/Ni[12] films with similar magnetic properties (anisotropy and magnetization values) are typically one order of magnitude higher. The lnv vs. $H^{-1/4}$ dependence is consistent with the propagation of a 1-D domain wall in a 2D weak random disorder.[3,21,22] It is worth noting that the slope given by $\beta U_c H_{dep}^{1/4}$ is slightly reduced for annealed samples of a given composition, which shows an increase of the energy barrier for DW motion.[3] This is consistent with depinning fields that are found (Table I) to be slightly higher for the annealed films. In ultra-thin magnetic films, the pinning potential corresponds to a distribution of magnetic anisotropy at the nanometer scale,[3,21] and this distribution may vary from amorphous to crystalline films as
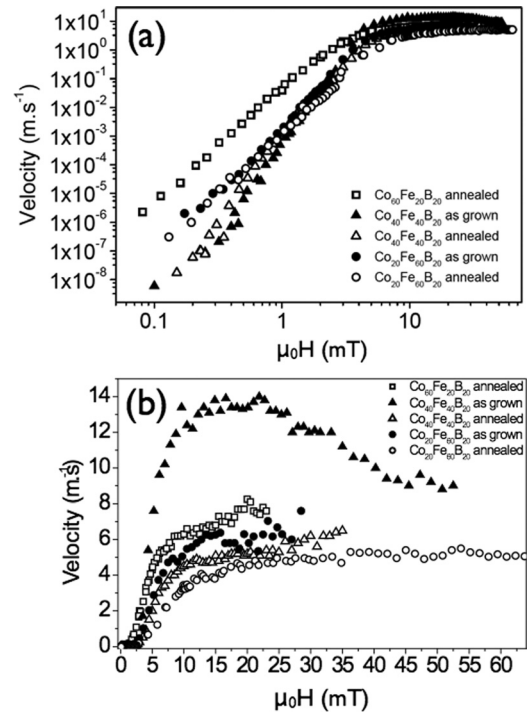

FIG. 3. (a) Domain wall velocity versus applied magnetic field on a logarithmic scale for compositions $Co_{20}Fe_{60}B_{20}$ as deposited (full dots) and after annealing (open dots), $Co_{40}Fe_{40}B_{20}$ as deposited (full triangle) and after annealing (open triangle), and $Co_{60}Fe_{20}B_{20}$ after annealing (open square). (b) High fields domain wall velocity for compositions of Fig. 3(a).

the average PMA increases. X-ray reflectivity studies and ToF-SIMS analysis show very low interface roughness <0.3 nm and intermixing in all the CoFeB films studied here but with a slight increase for annealed samples. Also, the presence of grain boundaries and crystalline texture in annealed CoFeB films may give rise to additional pinning. However, since H_{dep} also depends on magnetic parameters[3,21] such as the anisotropy and M_s values, it is difficult to give a final conclusion to the slight variation observed here. Finally, the low interface roughness, the low density of grain boundaries, and the better structural coherence in amorphous and fully crystallized CoFeB films as compared with fcc textured films such as Co/Pt, Co/Pd, or Co/Ni having similar magnetic properties could explain the low values of H_{dep}.

The high field dependence of the wall velocity for the different composition and crystalline states are shown in Fig. 3(b). For four of the systems considered, above the depinning field H_{dep}, the wall velocity increases almost linearly as a function of field up to a field H_{flo}, which is between 6 and 12.5 mT (see Table I). Above H_{flo}, the velocity reaches a plateau. The only exception involves as deposited samples of composition $Co_{40}Fe_{40}B_{20}$ as deposited, where a broad peak in the velocity is observed above H_{flo}. Moreover, we observed that the DW velocity (the high mobility regime slope and the maximum velocity) is slightly higher for the as-grown case than the annealed case for compositions $Co_{40}Fe_{40}B_{20}$ and $Co_{20}Fe_{60}B_{20}$.

In the following, we discuss about the origin of the two high fields motion regimes beyond the creep region, i.e., (i) $H_{dep} < H < H_{flo}$ and (ii) $H > H_{flo}$. In the flow regime motion, the 1D model predicts[4,5] a steady and precessional linear
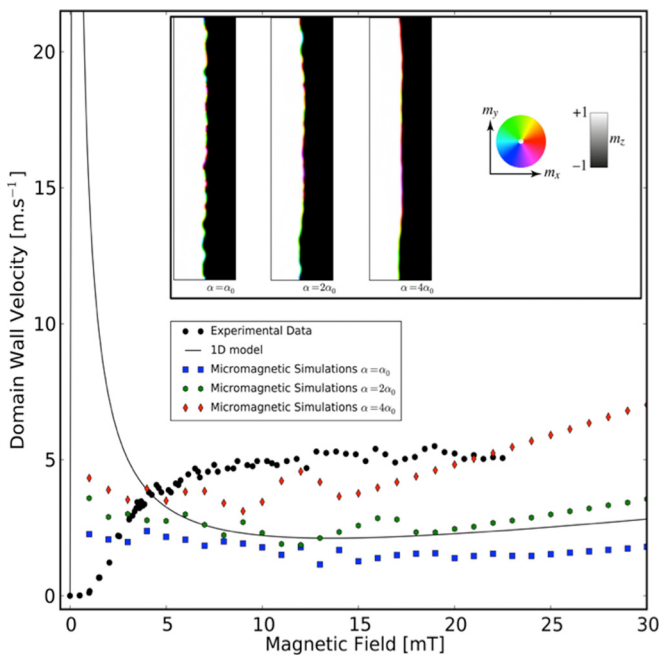
FIG. 4. Comparison of the measured DW velocities to the 1D model and micromagnetic simulations for the $Co_{60}Fe_{20}B_{20}$ composition after annealing. The negative DW differential mobility corresponds to the intermediate Walker regime above H_W. In the inset, different examples of micromagnetic states of the DW at 10 mT are presented for the different damping parameter values used in the micromagnetic simulations.

regimes separated by the Walker field H_W. From the material parameters in Table I, it is possible to evaluate the theoretical Walker field H_W. To compute the Walker field, we use the relation[23] $H_W = N_y M_S \alpha/2$, where N_y is the demagnetizing factor across the wall given as $(t_{CoFeB}/t_{CoFeB} + \Delta)$ and Δ is the domain wall width that can be calculated as $\Delta = (A/K_{eff} + N_y\mu_0 M_s^2/2)^{1/2}$. The low value of the damping parameters in our films leads to very low values of the Walker field H_W ranging from 0.3 to 0.8 mT, which are 50 times lower that those of Co/Pt films.[4] As a result of such low values, the Walker breakdown field lies inside the creep regime, i.e., $H_w \ll H_{dep}$, and is masked by the creep process. The intermediate regime $H_{dep} < H < H_{flo}$, which exhibits a very low wall mobility, is likely a transitory thermally activated depinning regime with a linear energy barrier consistent with theoretical predictions.[3,4,21] Note that H_{flo} is slightly higher for annealed films, which again indicate more pinning in the crystalline state.

The velocity plateau above the depinning transition corresponds to the low mobility regime above Walker breakdown. In Fig. 4(a), comparison of the experimental data for the $Co_{60}Fe_{20}B_{20}$ annealed sample with the 1D model and micromagnetics simulations is given. As the results from the 1D model show, the dynamics in the range of fields studied is expected to correspond to a precessional motion of the magnetization at the wall center, which leads to an overall wall velocity that is low and largely independent of the applied field. This behavior has been confirmed with micromagnetics simulations performed with the MuMax code.[24] The simulation geometry consists of a rectangular element with dimensions of $1280 \times 5120 \times 1$ nm, which is meshed using $256 \times 1024 \times 1$ finite difference cells along the (x,y,z) directions. The domain wall profile

extends along the y direction of the simulation rectangle to mimic as closely as possible the extended wall structures observed experimentally. The simulation grid is then shifted along the x-axis as the wall propagated along this direction, ensuring that the average wall center remained at the center of the simulation grid. For each applied field value, the simulation is run for 100 ns, but only the last 50 ns are used to determine the average wall velocity (in order to avoid transient dynamics). For the different Gilbert damping constants considered, transverse instabilities[6] in the wall structure are found to occur in the plateau at low applied fields (inset to Fig. 4), while at larger applied fields, the wall structure becomes more stable and a coherent magnetization precession is observed across the entire wall structure, which results in the linear increase in the wall velocity with applied field.

In conclusion, the possibility to use CoFeB thin films with very weak intrinsic pinning highlights a path toward the realization of magnetic shift memories where multiple DWs can move synchronously.

[1]S. S. P. Parkin, M. Hayashi, and L. Thomas, Science **320**, 190 (2008).
[2]A. Brataas, A. D. Kent, and H. Ohno, Nature Mater. **11**, 372 (2012).
[3]D. Ravelosona, "Domain wall dynamics," in *Nanoscale Materials and Applications* (Springer-Verlag, New York, 2009).
[4]P. J. Metaxas, J. P. Jamet, A. Mougin, M. Cormier, J. Ferré, V. Baltz, B. Rodmacq, B. Dieny, and R. L. Stamps, Phys. Rev. Lett. **99**, 217208 (2007).
[5]N. L. Schryer and L. R. Walker, J. Appl. Phys. **45**, 5406 (1974).
[6]K. Yamada, J. P. Jamet, Y. Nakatani, A. Mougin, A. Thiaville, T. Ono, and J. Ferré, Appl. Phys. Express **4**, 113001 (2011).
[7]A. P. Mihai, J. P. Attané, L. Vila, C. Beigné, J. C. Pillet, and A. Marty, Appl. Phys. Lett. **94**, 122509 (2009).
[8]C. Burrowes, D. Ravelosona, C. Chappert, S. Mangin, E. E. Fullerton, J. A. Katine, and B. D. Terris, Appl. Phys. Lett. **93**, 172513 (2008).
[9]D. Ravelosona, F. Caysol, J. Wunderlich, H. W. Schumacher, C. Chappert, V. Mathet, J. Ferre, and J. P. Jamet, J. Magn. Magn. Mater. **249**, 170 (2002).
[10]D. Ravelosona, S. Mangin, J. A. Katine, E. E. Fullerton, and B. D. Terris, Appl. Phys. Lett. **90**, 072508 (2007).
[11]O. Boulle, J. Kimling, P. Warnicke, M. Kläui, U. Rüdiger, G. Malinowski, H. J. M. Swagten, B. Koopmans, C. Ulysse, and G. Faini, Phys. Rev. Lett. **101**, 216601 (2008).
[12]C. Burrowes, A. P. Mihai, D. Ravelosona, J.-V. Kim, C. Chappert, L. Vila, A. Marty, Y. Samson, F. Garcia-Sanchez, L. D. Buda-Prejbeanu, I. Tudosa, E. E. Fullerton, and J.-P. Attané, Nat. Phys. **6**, 17 (2010).
[13]S. Ikeda, K. Miura, H. Yamamoto, K. Mizunuma, H. D. Gan, M. Endo, S. Kanai, J. Hayakawa, F. Matsukura, and H. Ohno, Nature Mater. **9**, 721 (2010).
[14]S. S. P. Parkin, C. Kaiser, A. Panchula, P. M. Rice, B. Hughes, M. Samant, and S.-H. Yang, Nature Mater. **3**, 862 (2004).
[15]S. Fukami, T. Suzuki, Y. Nakatani, N. Ishiwata, M. Yamanouchi, S. Ikeda, N. Kasai, and H. Ohno, Appl. Phys. Lett **98**, 82504 (2011).
[16]R. Mantovan, A. Lamperti, G. Tallarida, L. Baldi, M. Mariani, B. Ocker, S.-M. Ahn, I. Barisic, and D. Ravelosona, Thin Solid Films **533**, 75 (2013).
[17]A. Lamperti, S.-Min Ahn, B. Ocker, R. Mantovan, and D. Ravelosona, Thin Solid Films **533**, 79 (2013).
[18]K. Lee, J. J. Sapan, S. H. Kang, and E. E. Fullerton, J. Appl. Phys. **109**, 123910 (2011).

[19]M. Munaka, S.-I. Aoqui, and M. Yagi, IEEE. Trans. Magn. **41**, 3262 (2005).

[20]T. Devolder, P.-H. Ducrot, J.-P. Adam, I. Barisik, N. Vernier, J.-Von Kim, B. Ockert, and D. Ravelosona, Appl. Phys. Lett. **102**, 022407 (2013).

[21]J. Ferré, *Dynamics of Magnetization Reversal: From Continuous to Patterned Ferromagnetic Films* (Springer-Verlag, Berlin, 2002).

[22]F. Cayssol, D. Ravelosona, C. Chappert, J. Ferré, and J. P. Jamet, Phys. Rev. Lett. **92**, 107202 (2004).

[23]A. Mougin, M. Cormier, J. P. Adam, P. J. Metaxas, and J. Ferré, Europhys. Lett. **78**, 57007 (2007).

[24]A. Vansteenkiste and B. Van de Wiele, J. Magn. Magn. Mater. **323**, 2585 (2011).